Article

The Tetramerization Domain Potentiates Kv4 Channel Function by Suppressing Closed-State Inactivation

Yi-Quan Tang,[1] Jing-Heng Zhou,[1] Fan Yang,[2] Jie Zheng,[2] and KeWei Wang[1,3,*]
[1]Department of Molecular and Cellular Pharmacology, State Key Laboratory of Natural and Biomimetic Drugs, Peking University School of Pharmaceutical Sciences, Beijing, China; [2]Department of Physiology and Membrane Biology, University of California School of Medicine, Davis, California; and [3]PKU-IDG/McGovern Institute for Brain Research, Peking University, Beijing, China

ABSTRACT A-type Kv4 potassium channels undergo a conformational change toward a nonconductive state at negative membrane potentials, a dynamic process known as pre-open closed states or closed-state inactivation (CSI). CSI causes inhibition of channel activity without the prerequisite of channel opening, thus providing a dynamic regulation of neuronal excitability, dendritic signal integration, and synaptic plasticity at resting. However, the structural determinants underlying Kv4 CSI remain largely unknown. We recently showed that the auxiliary KChIP4a subunit contains an N-terminal Kv4 inhibitory domain (KID) that directly interacts with Kv4.3 channels to enhance CSI. In this study, we utilized the KChIP4a KID to probe key structural elements underlying Kv4 CSI. Using fluorescence resonance energy transfer two-hybrid mapping and bimolecular fluorescence complementation-based screening combined with electrophysiology, we identified the intracellular tetramerization (T1) domain that functions to suppress CSI and serves as a receptor for the binding of KID. Disrupting the Kv4.3 T1-T1 interaction interface by mutating C110A within the C3H1 motif of T1 domain facilitated CSI and ablated the KID-mediated enhancement of CSI. Furthermore, replacing the Kv4.3 T1 domain with the T1 domain from Kv1.4 (without the C3H1 motif) or Kv2.1 (with the C3H1 motif) resulted in channels functioning with enhanced or suppressed CSI, respectively. Taken together, our findings reveal a novel (to our knowledge) role of the T1 domain in suppressing Kv4 CSI, and that KChIP4a KID directly interacts with the T1 domain to facilitate Kv4.3 CSI, thus leading to inhibition of channel function.

INTRODUCTION

Voltage-gated K^+ (Kv) channels close rapidly during sustained depolarization by a dynamic process known as inactivation (the nonconductive state), which is essential for channel function and modulation of membrane excitability. Inactivation can occur from the open state at strongly depolarized membrane potentials (known as open-state inactivation (OSI)) or from pre-open closed states (known as closed-state inactivation (CSI)) at hyperpolarized and modestly depolarized membrane potentials (1). The Kv4 channel, however, exhibits a unique inactivation gating property that distinguishes it from other rapidly inactivating Kv channels, since its midpoint of steady-state inactivation (SSI) is typically below the potential at which channels are activated and close to the resting membrane potential of neurons, indicating a preferential CSI in Kv4 channels (1–3). When functionally coupled with subthreshold excitatory postsynaptic potentials (EPSPs), this preferential CSI causes inhibition of Kv4 channel activity without requiring channel opening. Thus, A-type Kv4 currents (I_A) play a unique role in regulating neuronal excitability, dendritic signal integration, and synaptic plasticity in the postsynaptic compartments where the channels are localized (4–9). Despite the importance of CSI in determining membrane excitability, the structural determinants underlying Kv4 CSI remain largely unknown.

The cytoplasmic N-terminal tetramerization domain (T1) of Kv channels is positioned beneath the bundle crossing of four transmembrane S6 segments that constitute the main activation gate (10). The Kv4 T1 domain features an intersubunit Zn^{2+}-binding motif (C3H1 motif, $HX_5CX_{20}CC$) that is highly conserved among *non-Shaker*-type (Kv2-4) channels (11,12). The structure of the T1 domain comprises four Zn^{2+} ions bound at the T1-T1 intersubunit interface, and each interfacial Zn^{2+} ion is coordinated by a cysteine from one subunit and a histidine along with two cysteines from the neighboring subunit (11,13). Although the T1 domain primarily functions to mediate channel tetramerization, it also plays a significant role in channel gating (14–17) and association of auxiliary cytoplasmic β subunits for diverse modulation of inactivation (13,18).

Among the intracellular factors that affect Kv4 inactivation gating, cytosolic Kv channel-interacting proteins (KChIPs) are the best-studied Kv4 auxiliary subunits that share a conserved C-terminal core and a variable N-terminal domain (19). The cocrystal structure of the Kv4.3 N-terminus/KChIP1 complex reveals that the KChIP core sequesters the proximal N-terminus of one Kv4.3 subunit and binds to the adjacent T1 domain of another Kv4.3 subunit, forming a clamp to stabilize the tetrameric assembly of Kv4 channels

Submitted February 12, 2014, and accepted for publication July 1, 2014.
*Correspondence: wangkw@hsc.pku.edu.cn or wangkw@bjmu.edu.cn
Editor: William Kobertz.
© 2014 by the Biophysical Society
0006-3495/14/09/1090/15 $2.00
http://dx.doi.org/10.1016/j.bpj.2014.07.038

(20,21), whereas the variable N-terminus of KChIPs has been shown to induce diverse modulation of Kv4 function (22–25). KChIP4a, a KChIP4 splice variant, exhibits distinct modulation of Kv4 channel gating and surface expression via its unique N-terminus (22,26). We recently showed that the N-terminal Kv4 inhibitory domain (KID) of KChIP4a exerts an inhibitory effect on channel gating by promoting CSI (27). Thus, the N-terminal KID of KChIP4a can be utilized as a probe to identify structural and functional elements critical for Kv4 CSI.

In this study, we found that the T1 domain plays a critical role in suppressing Kv4 CSI and serves as a receptor for binding of the auxiliary KChIP4a N-terminus that enhances Kv4.3 CSI. Therefore, we propose that the T1-T1 intersubunit interface, consisting of the C3H1 motif, functions to prevent the A-type Kv4 channel from entering CSI, thereby facilitating Kv4 channel function.

MATERIALS AND METHODS

Molecular biology

All restriction enzymes and T4 DNA ligase were purchased from Takara. All point mutants, deletion mutants, and fusion proteins were created by PCR-based mutagenesis strategies with LA taq or PrimeSTAR HS DNA Polymerase (Takara). For two-hybrid fluorescence resonance energy transfer (FRET) mapping experiments, the following sequences were cloned into the *Eco*RI and AgeI restriction sites of pECFP-N1 or pEYFP-N1 vector (Clontech):

KID (MNLEGLEMIAVLIVIVLFVKLLEQFGLIEAGLED)

S1 (ALVFYYVTGFFIAVSVITNVV)

S4-S5 (VTLRVFRVFRIFKFSRHSQGLRILGYTLKSCASELGFLLFSLTMAIIIFATVMFY)

S6-10 (IFGSICSLSGVLVIALPVPVIVSNFSRIYHQ)

S6-60 (IFGSICSLSGVLVIALPVPVIVSNFSRIYHQNQRADKRRAQKKARLARIRVAKTGSSNAYLHSKRNGLLNEALELTGTPEE)

T1 (DELIVLNVSGRRFQTWRTTLERYPDTLLGSTEKEFFFNEDTKEYFFDRDPEVFRCVLNFYRTGKLHYPRYECISAYDDELAFYGILPEIIGDCCYEEYKDRKRENAE)

T1-C110A (DELIVLNVSGRRFQTWRTTLERYPDTLLGSTEKEFFFNEDTKEYFFDRDPEVFRCVLNFYRTGKLHYPRYEAISAYDDELAFYGILPEIIGDCCYEEYKDRKRENAE)

For bimolecular fluorescence complementation (BiFC)-based screening, the KID, S1, S4-S5, S6-10, S6-60, T1, and T1-C110A sequences were cloned into the *Hin*dIII and SalI restriction sites of pBiFC-VN173 (residues 1–173 of Venus) vector or the *Eco*RI and KpnI restriction sites of pBiFC-VC155 (residues 155–238 of Venus) vector. For surface biotinylation, KChIP4a, KChIP4aΔ34, Kv4.3, and Kv4.3 C110A mutants were cloned into the XhoI and *Eco*RI restriction sites of pcDNA3.1 (−) vector. For electrophysiological recordings in *Xenopus* oocytes, Kv4.3, Kv4.3Δ24, Kv4.3 C110A, Kv4.3 C110AΔ24, Kv4.3-T1(Kv1.4), Kv4.3Δ24-T1(Kv1.4), Kv4.3Δ24-T1(Kv2.1), KChIP4a, KChIP4aΔ34, and KChIP4a 19-22A were subcloned into the SalI and *Eco*RI restriction sites of pBluescript KSM vector.

Two-electrode voltage-clamp recordings in *Xenopus* oocytes

All cRNAs were transcribed in vitro using the T3 mMESSAGE mMACHINE T3 Kit (Ambion) following linearization of cDNAs with NotI. *Xenopus laevis* oocytes (stage V-VI) were selected and injected with 46 nl of solution containing 0.5–5.0 ng of selected cRNA using a microinjector (Drummond Scientific). Oocytes were incubated in ND96 solution (96 mM NaCl, 2 mM KCl, 1.8 mM $CaCl_2$, 1 mM $MgCl_2$, 5 mM HEPES, pH 7.4, adjusted with NaOH) at 17°C for 24–48 hr. Two-electrode voltage-clamp recordings were conducted in ND-96 solution at room temperature (22°C ± 1°C) using a GeneClamp 500B amplifier (Axon Instruments). The tip resistance of borosilicate pipettes filled with 3 M KCl was typically 0.5–1.0 MΩ. Data were acquired using PatchMaster software (HEKA Electronics) and digitized at 1 kHz with an LIH 8+8 (HEKA Electronics). OriginPro 8.6 (OriginLab) was used to analyze the data.

The voltage-clamp protocols and analyses used in this investigation were similar to those employed in our recent KChIP4a studies (27). To measure the peak current amplitudes, the currents were evoked by a 2 s depolarizing pulse to +40 mV from a holding potential of −100 mV. CSI was measured by a double-pulse protocol with a conditioning pulse at −50 mV, −60 mV, or −70 mV in variable durations (Δt) of 5 ms to 10.4 s. The current amplitudes evoked by the second pulse (+40 mV) in the protocol, relative to the amplitudes resulting from the first control pulse (I_{post}/I_{pre}), were plotted as a function of different durations of the conditioning pulses. For recovery from inactivation and recovery from CSI, currents were recorded at +40 mV with a specialized double-pulse protocol. CSI was induced at −70 mV, −60 mV, or −50 mV for 5 s, and recovery was measured at −100 mV for variable durations (Δt). The current amplitudes evoked by the postpulse, normalized to the amplitudes obtained by the initial control pulse, were plotted against the interpulse duration. The kinetics of CSI, recovery from inactivation, and recovery from CSI were obtained by fitting with a single-exponential function. The SSI protocol consisted of a 1, 5, or 10 s prepulse stepped from −120 mV to 0 mV in 10 mV increments, followed by a test pulse of +40 mV. The fraction of available current (I/I_{max}) was plotted against the prepulse potentials. The peak conductance-voltage (G-V) relationship was derived from peak current amplitudes evoked by depolarizing steps from −100 mV to +60 mV at 10 mV increments. The calculation was based on the equation $G = I/(V - V_{rev})$, where I is the peak current amplitude at the test potential V, and V_{rev} is the reversal potential. The voltage dependence of steady-state activation (G/G_{max}) and inactivation (I/I_{max}) was fitted to the following single Boltzmann relationship: $y = 1/\{1 + \exp[(V - V_{1/2})/k]\}$, where V is the test potential, $V_{1/2}$ is the potential for half-maximal activation or inactivation, and k is the corresponding slope factor. All holding potentials were −100 mV in this study unless specified.

FRET and BiFC assays

HEK293T cells were maintained in Dulbecco's modified Eagle's medium (Invitrogen) with 10% fetal bovine serum (HyClone) at 37°C under 5% CO_2. For FRET experiments, cells were reseeded on glass coverslips coated with poly-D-lysine and transfected using Lipofectamine 2000 (Invitrogen) according to the manufacturer's instructions. At 24–48 hr posttransfection, the cells were washed twice with phosphate-buffered saline (PBS) containing 1 mM $MgCl_2$ and 0.1 mM $CaCl_2$, and fixed in 4% paraformaldehyde at 4°C for 15 min. Images were obtained using a confocal microscope (FV1000; Olympus). FRET was measured from donor dequenching upon acceptor photobleaching. CFP and YFP were excited at 456 nm and 515 nm, respectively. The emission intensities of CFP before and after photobleaching of YFP within the region of interest (indicated by white boxes (see Fig. 2 B, C, and D and Fig. 7 A and B)) were compared and used to calculate FRET efficiency with the use of Olympus Fluoview FV1000 analysis software. The distance (R) between donor and acceptor was calculated as $R = R_0 \times [(1/E) - 1]^{1/6}$, where R_0 (5.3 nm) is the Förster critical distance when the donor is ECFP and the acceptor is EYFP, and E represents FRET efficiency $E = (1 - F_D/F_D')$, in which F_D and F_D' are the donor fluorescence intensity before and after acceptor bleaching, respectively.

For BiFC experiments, HEK293T cells were cotransfected with N- and C-terminal Venus plasmids that were modified to contain Kv4 channel peptides or KID. At 24 h posttransfection, the cells were imaged by confocal fluorescent microscopy as described above. Venus was excited at 515 nm.

To quantify BiFC, HEK293T cells were transfected with 1 μg of each BiFC construct per 35 mm dish, and 0.5 μg mCherry plasmid was cotransfected per transfection as an internal control. The transfected cells were harvested ~24 hr posttransfection. The cells were washed twice with 1 ml of filtered 1× PBS and resuspended in 500 μl 1× filtered PBS. The cells were then filtered using a 5 ml polystyrene round-bottom tube with a cell-strainer cap (12 × 17 mm style; BD Falcon) and analyzed by flow cytometry (BD FACSAria III). To quantify the amount of complementation, we analyzed both $Venus^+$ and $mCherry^+$ cells and determined the percentage of $mCherry^+$ cells that were $Venus^+$.

Western blot analysis

HEK293T cells transfected with indicated plasmids were lysed with lysis buffer (150 mM NaC1, 20 mM Tris, 1% Triton X-100, 1% sodium deoxycholate, 0.1% SDS, 10 mM EDTA, and proteinase inhibitor mixture (Roche), pH 8.0) for 30 min on ice. Cell lysates were then centrifuged at 4°C for 10 min at 13,000 rpm. The protein concentration in the supernatant was determined with the BCA protein assay kit (Pierce). Protein samples were then separated by running on an 8% SDS-PAGE gel and transferred electrophoretically to nitrocellulose membranes (Millipore). After blocking in 1X-TBST containing 5% skim milk, nitrocellulose membranes were incubated with mouse monoclonal anti-Kv4.3 (1:2000; Abcam), rabbit polyclonal anti-actin (1:500; Santa Cruz), or mouse monoclonal anti-transferrin receptor (1:500; Invitrogen) antibody at 4°C overnight. The membranes were then incubated with their corresponding secondary horseradish peroxidase-conjugated antibodies and detected using the ECL western blotting detection system (Millipore).

Cell-surface biotinylation assay

Surface biotinylation of transfected HEK293T cells was completed as previously described (27). Briefly, the transfected HEK293T cells were washed three times with ice-cold D-PBS (PBS containing 0.5 mM $MgCl_2$ and 1 mM $CaCl_2$), followed by incubation with D-PBS containing 0.5 mg/ml EZ-Link Sulfo-NHS-SS-biotin (Pierce) for 1 h on ice to biotinylate cell-surface proteins. Excess biotin was quenched with TBS containing 100 mM glycine. The cell lysates were prepared and divided into two fractions (one for measuring total protein and the other for surface proteins), and isolated by affinity purification of biotinylated proteins with NeutrAvidin-conjugated agarose beads (Pierce). The total and surface proteins were both subjected to western blot analysis as described above.

RESULTS

The N-terminal KID of KChIP4a promotes CSI of Kv4.3

We recently showed that the distinct N-terminal KID of KChIP4a (residues 1–34) differentially regulates the open state and CSI of Kv4 channels (27). To investigate the molecular mechanism underlying KChIP4a N-terminal KID-mediated modulation of Kv4 gating, we recorded currents of Kv4.3 channels coexpressed with auxiliary KChIP4a in *Xenopus* oocytes. Coexpression of Kv4.3 with wild-type KChIP4a resulted in enhanced CSI, whereas the N-terminal KID truncation (KChIP4aΔ34) or alanine substitutions of residues 19–22 (KChIP4a 19-22A) drastically slowed CSI (Fig. 1, A and B; Table S1 in the Supporting Material), suggesting that residues 19–22 within the KID bind to Kv4 channels to promote CSI (27). Further analysis of CSI at different prepulse voltages (−70 mV, −60 mV, and −50 mV) confirmed the role of the KID in promoting Kv4.3 channel CSI (Fig. S1, A–C). An examination of the voltage dependence of SSI revealed that inactivation of Kv4.3 was prominently coupled to the closed states, as indicated by the activation threshold (~−40 mV), and the KID caused a hyperpolarized shift in SSI curves in a prepulse-duration-dependent manner (Fig. S1, D–F; Table S2).

Because Kv channels spontaneously undergo an interconversion back to the conductive state (recovery) from the nonconductive state (inactivation), we also analyzed the rate of recovery from either inactivation or CSI. The recovery rate was significantly accelerated by KChIP4aΔ34 or KChIP4a 19-22A, but was not affected by wild-type KChIP4a (Figs. 1, C–G, and S2), indicating that the KID retarded recovery from both inactivation and CSI, which is the opposite of the effect observed for the KChIP4a core (KChIP4aΔ34). These results demonstrate that the N-terminal KID of KChIP4a promotes Kv4.3 CSI that is coupled with the slowed recovery from inactivation.

The N-terminal KID of KChIP4a directly interacts with the T1 domain of Kv4.3 channels

To probe for the site that is critical for KChIP4a KID binding to Kv4.3, we used a FRET-based peptide hybridization assay (28) and generated short channel peptides that included S4 (voltage sensor), the S4-S5 linker, S6, and the post-S6 segment (activation gate), based on previously reported structural correlates for Kv4 CSI (29–32). Each peptide segment was fused with a YFP, yielding a series of prey constructs that could be pitted against the CFP-tagged KID (KID-CFP) as a bait (Fig. 2 *A*), with the T1-T1 interaction pair as a positive control (Fig. 2 *B*).

After photobleaching of YFP in cells coexpressing T1-CFP and T1-YFP, the fluorescence of CFP in the corresponding region (indicated by the *white frame* in Fig. 2 *B*) was enhanced. FRET efficiency increased inversely with the relative ratio of donor (D) to acceptor (A) (D/A ratio; $R^2 = 0.154$; Fig. 3 *A*) and was not correlated with the absolute level of acceptor emission (A level; $R^2 = 0.0036$; Fig. 3 *B*), suggesting a direct protein-protein interaction instead of random association.

We coexpressed individual pairs of bait and prey constructs, and probed for FRET between CFP and YFP in HEK293T cells. FRET signal was observed for the KID and T1 pair, but there was a lack of interaction between KID and S1 (Fig. 2, *C* and *D*). For the KID and T1 pair, FRET efficiency also increased as the D/A ratio decreased ($R^2 = 0.19$; Fig. 3 *C*), but was not correlated with the amount of acceptor ($R^2 = 0.0176$; Fig. 3 *D*). Quantitative analysis revealed that the FRET efficiency value was 0.132 ± 0.007 for the T1 + T1 pair, and 0.102 ± 0.006 for the KID + T1 pair (Fig. 2 *E*). Pairing of KID + S4-S5 gave an average value of 0.041 ± 0.009, implying a weak

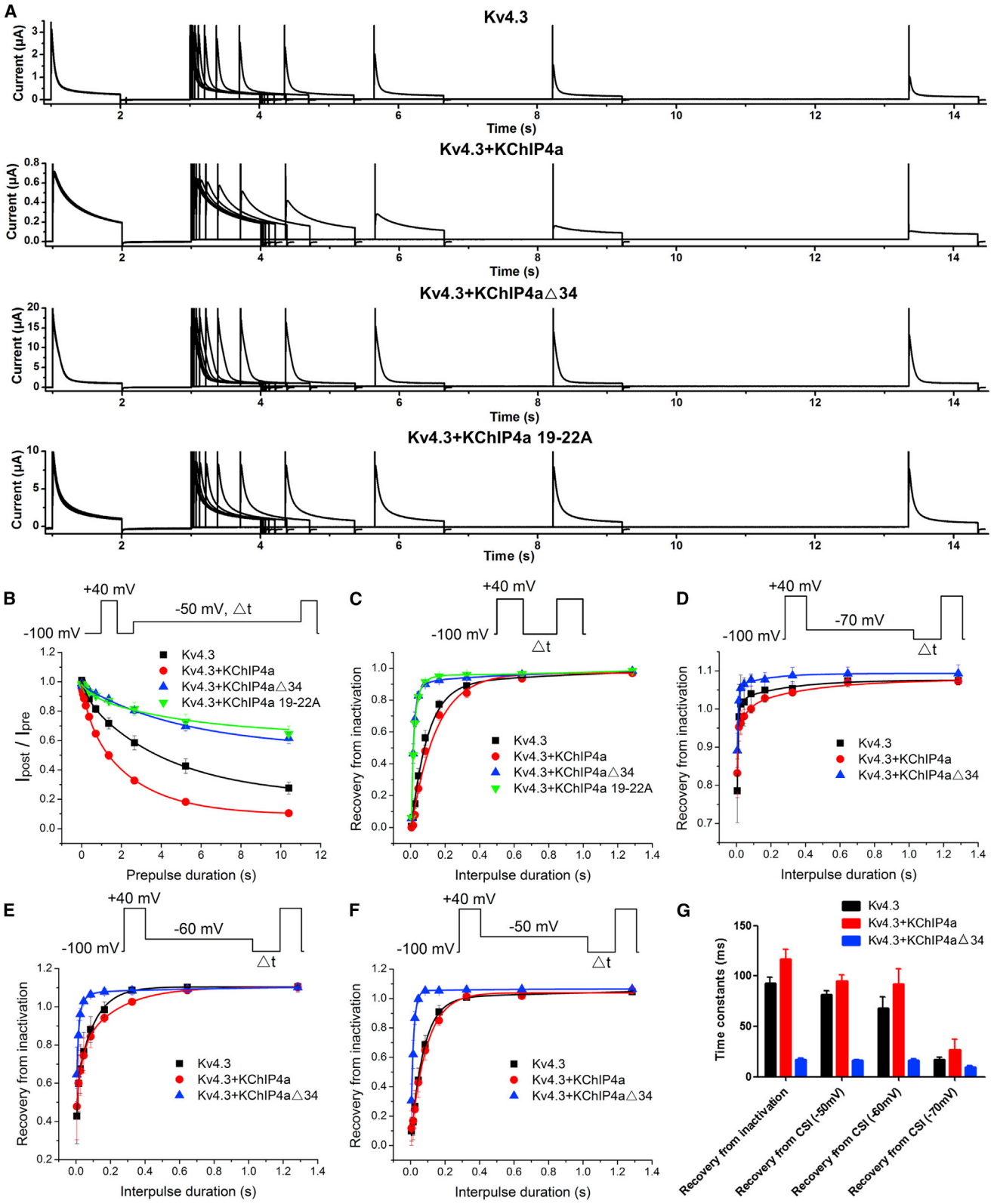

FIGURE 1 The N-terminal KID of KChIP4a promotes CSI of Kv4.3 channels. (*A*) Representative current traces of CSI from oocytes expressing Kv4.3, Kv4.3+KChIP4a, Kv4.3+KChIP4aΔ34, or Kv4.3+KChIP4a 19-22A. Currents were recorded at +40 mV using a double-pulse protocol with a conditioning pulse at −50 mV in variable durations (Δt) of 5 ms to 10.4 s. The current amplitudes evoked by the second pulse (+40 mV) in the protocol, relative to the amplitudes resulting from the first control pulse (I_{post}/I_{pre}), were plotted as a function of different durations of the conditioning pulses. (*B*) CSI curve for Kv4.3, Kv4.3+KChIP4a, Kv4.3+KChIP4aΔ34, or Kv4.3+KChIP4a 19-22A. (*C*) Recovery from inactivation for Kv4.3, Kv4.3+KChIP4a,

(legend continued on next page)

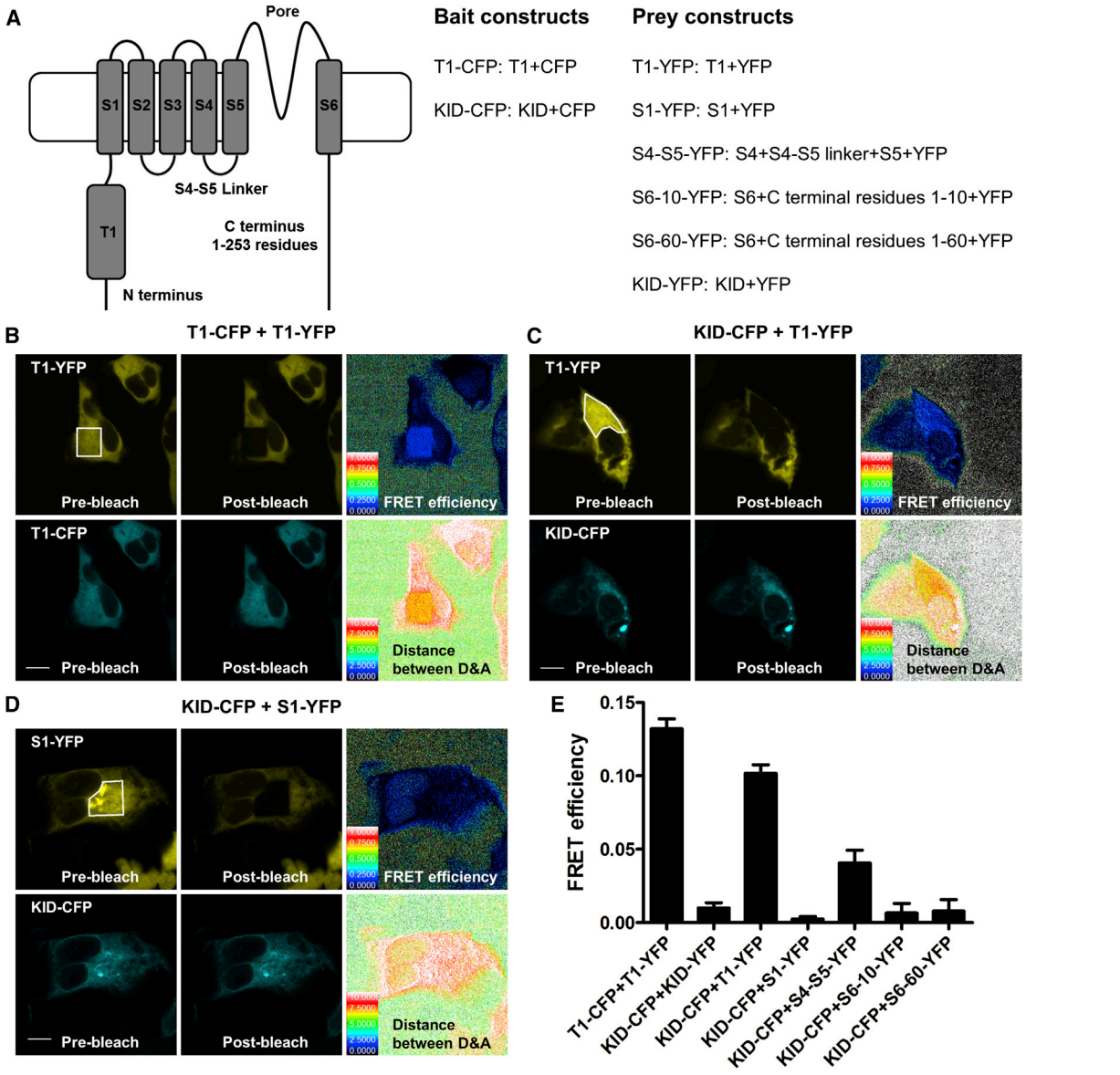

FIGURE 2 Identification of the Kv4.3 T1 domain responsible for KID binding by FRET two-hybrid mapping. (*A*) Schematic presentation of Kv4.3, CFP-tagged bait constructs, and YFP-tagged prey constructs. (*B*) Visualization of FRET in HEK293T cells transfected with T1-CFP and T1-YFP. Images were obtained by excitation at 515 nm for YFP fluorescence (*upper-left and middle panels*) or at 456 nm for CFP fluorescence (*lower-left and middle panels*). In the upper-left panel, the region selected for photobleaching is indicated by white boxes. The upper-right panel indicates FRET efficiency and the lower-right panel indicates the distance between the donor and the acceptor. (*C* and *D*) Visualization of FRET in HEK293T cells transfected with KID-CFP and T1-YFP (*C*) or KID-CFP and S1-YFP (*D*). (*E*) Quantitative analysis of FRET efficiency between CFP-tagged bait and YFP-tagged prey. The scale bar represents 10 μm. To see this figure in color, go online.

association between these two components (Fig. 2 *E*). In contrast, FRET was absent for the other four analyzed protein pairs (KID + KID, KID + S1, KID + S6-10, and KID + S6-60; Figs. 2 *E* and S3).

To further confirm the interaction, we also used a BiFC-based screening assay to evaluate the associations between the KID and Kv4.3 channel fragments/peptides. The BiFC assay is based on the formation of a fluorescent complex

Kv4.3+KChIP4aΔ34, or Kv4.3+KChIP4a 19-22A. Mean normalized current amplitudes were plotted as a function of interpulse duration. (*D–F*) Recovery from CSI for Kv4.3, Kv4.3+KChIP4a, or Kv4.3+KChIP4aΔ34. Currents were recorded at +40 mV with a specific double-pulse protocol. CSI was induced at −70 mV (*D*), −60 mV (*E*), or −50 mV (*F*) for 5 s, and recovery was measured at −100 mV for variable durations (Δt). The current amplitudes evoked by the postpulse, normalized to the amplitudes obtained by the initial control pulse, were plotted against the interpulse duration. (*G*) Time constants of recovery from inactivation or CSI. A single-exponential function was used to fit the plotted data points for the recovery time constants. To see this figure in color, go online.

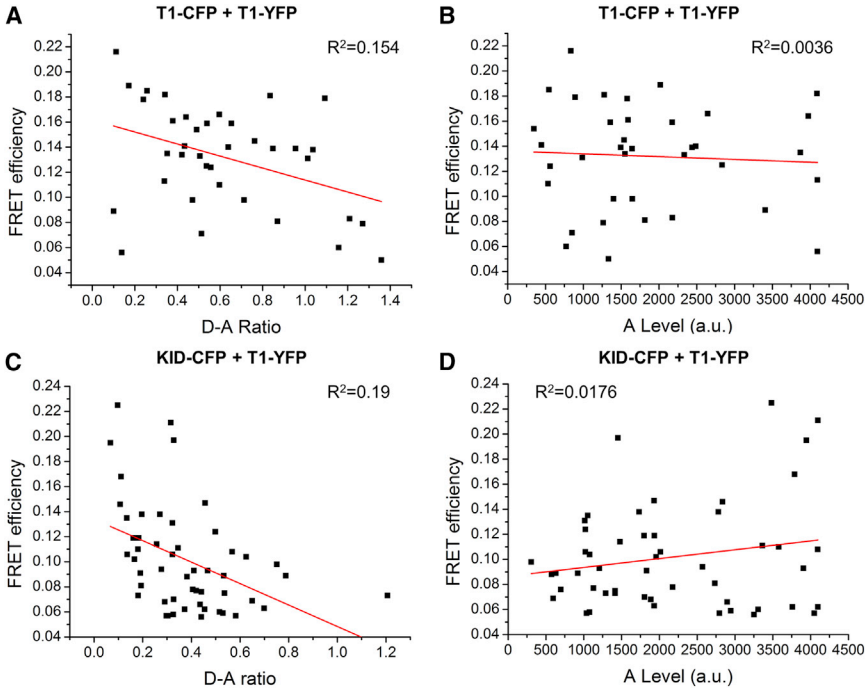

FIGURE 3 Direct interaction between the KID and the T1 domain of Kv4.3 measured by FRET. (*A–D*) FRET efficiency is plotted as a function of the relative concentration ratio of donor/acceptor (D/A ratio) or acceptor emission level (A Level (a.u.)) for different combinations. In cells coexpressing T1-CFP + T1-YFP (*A* and *B*) or KID-CFP + T1-YFP (*C* and *D*), FRET efficiency increased inversely with the D/A ratio, but was insensitive to the increase in the absolute acceptor level (A Level (a.u.)), indicating a direct interaction between donors and acceptors instead of random association. To see this figure in color, go online.

comprised of two nonfluorescent fragments of Venus (a highly fluorescent YFP mutant): VN173 (residues 1–173) and VC155 (residues 155–238). These fragments are brought together by the association of two interacting proteins, thus allowing for in situ detection of a wide variety of protein-protein interactions (Fig. 4 *A*) (33,34). The N-terminal VN173 or C-terminal VC155 fragments of Venus were fused to the C-terminus of the indicated proteins (Fig. 4 *A*), with the T1-T1 pair used as a positive control and the KID-KID pair used as a negative control.

Coexpression of T1-VN173 with T1-VC155 in HEK293T cells gave rise to strong yellow fluorescence. In contrast, coexpression of KID-VN173 with KID-VC155 resulted in no fluorescence emission (Fig. 4 *B*). When various combinations of the KID and Kv4.3 channel fragments were transfected, strong fluorescent signals were observed only in cells expressing KID-VN173 and T1-VC155 or T1-VN173 and KID-VC155, whereas weak fluorescent signals were observed in cells expressing KID-VN173 and S4-S5-VC155 or S4-S5-VN173 and KID-VC155 (Fig. 4 *B*), consistent with the FRET results (Fig. 2). Coexpression of the KID with S1, S6-10, or S6-60 yielded no clear fluorescence signals (Fig. 4 *B*), indicating a lack of interaction between them. To determine the BiFC efficiency, we performed a fluorescence-activated cell sorting (FACS) analysis of cells transfected with various Venus BiFC constructs and mCherry-expressing plasmid, and determined the proportions of $Venus^+$ cells in the transfected $mCherry^+$ cells (Fig. 4 *C*). Cotransfection with T1-VN173 and T1-VC155 reconstituted Venus fluorescence in 89% of the $mCherry^+$ cells (Fig. 4 *C*). Transfection with the T1-VN173 and KID-VC155 pair or the KID-VN173 and T1-VC155 pair resulted in reconstitution of Venus fluorescence with a similar efficiency (83% and 70%, respectively), indicating that interactions between the VN173 and VC155 fragments mediated by the KID and T1 were necessary to achieve efficient reconstitution of Venus fluorescence (Fig. 4 *C*). Reconstitution of Venus fluorescence between the KID-VN173 and S4-S5-VC155 pair or the S4-S5-VN173 and KID-VC155 pair was much less efficient (26% and 24%, respectively). When all other BiFC pairs were cotransfected, less than 10% of the cells expressing Venus fluorescence in $mCherry^+$ cells were observed (Fig. 4 *C*). These results from FRET and BiFC experiments demonstrated a direct interaction between the N-terminal KID of KChIP4a and the T1 domain of Kv4.3 channels.

Disrupting the T1-T1 interface abolishes the enhanced CSI induced by the KChIP4a KID

The T1 domain of the Kv4 channel contains a characteristic C3H1 motif. This motif is not a linear sequence ($HX_5CX_{20}CC$) and is composed of a cysteine from one subunit and a histidine along with two cysteines from the neighboring subunit (Fig. 5 *A*).

The C3H1 motif is positioned beneath the S6 bundle crossing and has been proposed to link voltage-dependent conformational changes of Kv4 channels (16,17). To test whether the T1 domain is critically involved in KChIP4a KID-mediated modulation of Kv4.3 channel gating, we generated a C110A mutation within the C3H1 motif of the T1 domain that disrupts T1-T1 interactions (Fig. 5 *A*)

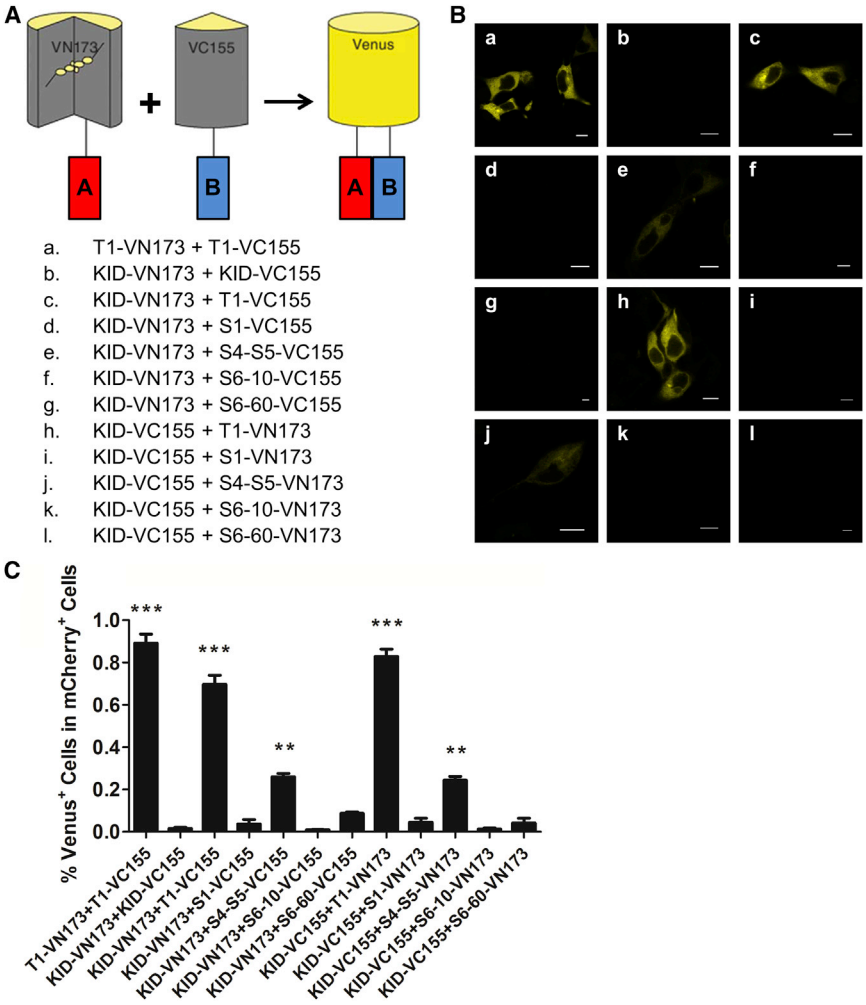

FIGURE 4 Identification of the Kv4.3 T1 domain responsible for KID binding by BiFC-based screening assay. (*A*) The principle of the Venus BiFC system and a schematic view of the fusion protein constructs used in this study. (*B*) HEK293T cells were transfected with BiFC expression vectors fused to the KID or the Kv4.3 channel peptides as indicated in *A*; cells were then analyzed for fluorescence after incubation at 37°C for 24 h. (*C*) Quantitative analysis of BiFC by flow cytometry. HEK293T cells were cotransfected with various Venus BiFC constructs and mCherry expression plasmid as an internal control for transfection, and the percentage of $Venus^+$ cells in $mCherry^+$ cells was determined. Data are representative of three independent experiments. $^{**}p < 0.01$; $^{***}p < 0.001$ compared with HEK293T cells transfected with KID-VN173 + S1-VC155. To see this figure in color, go online.

(35). Biochemical experiments showed that both the total and surface expression levels of the Kv4.3 C110A mutant coexpressed with KChIP4a (C110A/KChIP4a) or KChIP4aΔ34 (C110A/KChIP4aΔ34) were lower than those of wild-type Kv4.3 coexpressed with KChIP4a (Kv4.3/KChIP4a) or KChIP4aΔ34 (Kv4.3/KChIP4aΔ34) (Fig. 5, *B–D*). Electrophysiological recordings showed that the current amplitude of C110A/KChIP4aΔ34 was lower than that of Kv4.3/KChIP4aΔ34 (Fig. 5 *E*). Surprisingly, the current density for the C110A/KChIP4a channel complex, in contrast to the protein expression level, was much larger than that of Kv4.3/KChIP4a (Fig. 5 *E*). These results suggested that disrupting the T1-T1 interface by mutating C110A within the C3H1 motif abolished the enhanced Kv4.3 CSI induced by KChIP4a KID and prevented more channels from entering CSI, thus resulting in more channels in the open state. To test this notion, we measured the CSI kinetics of the C110A/KChIP4a channel complex. As expected, the CSI kinetics of C110A/KChIP4a was identical to that of C110A/KChIP4aΔ34 (Fig. 6, *A* and *B*; Table S1). We further confirmed effect by examining the voltage dependence of SSI, in which the hyperpolarizing shift of SSI induced by the KID was also completely disrupted by C110A mutation (Figs. 6 *C* and S4, A–C; Table S2). In contrast, the CSI and SSI curves of C110A/KChIP4aΔ34 were almost identical to that of Kv4.3/KChIP4aΔ34 (Figs. 6, *A–C*, and S4, A–C; Tables S1 and S2), suggesting that disrupting the C1H1 motif by the C110A mutation produced no effect on the regulatory function of KChIP4aΔ34. Consistently, C110A mutation also eliminated the KID-induced slow recovery from inactivation (Fig. 6 *D*). Steady-state activation was not significantly affected by C110A mutation upon coexpression with either KChIP4a or KChIP4aΔ34 (Fig. 6 *E*).

To further investigate whether the lack of KID-mediated CSI enhancement resulted from the dissociation between the KID and the mutated T1 domain, we coexpressed the KID and the T1 domain with C110A mutation, and probed for a FRET signal between CFP and YFP in HEK293T cells (Fig. 7). Surprisingly, the intracellular distribution pattern of the T1 domain was totally altered by C110A point mutation, switching from a perinuclear distribution to nucleus-enriched distribution (Fig. 7, *A* and *B*). In agreement with previous studies (35), C110A mutation disrupted the

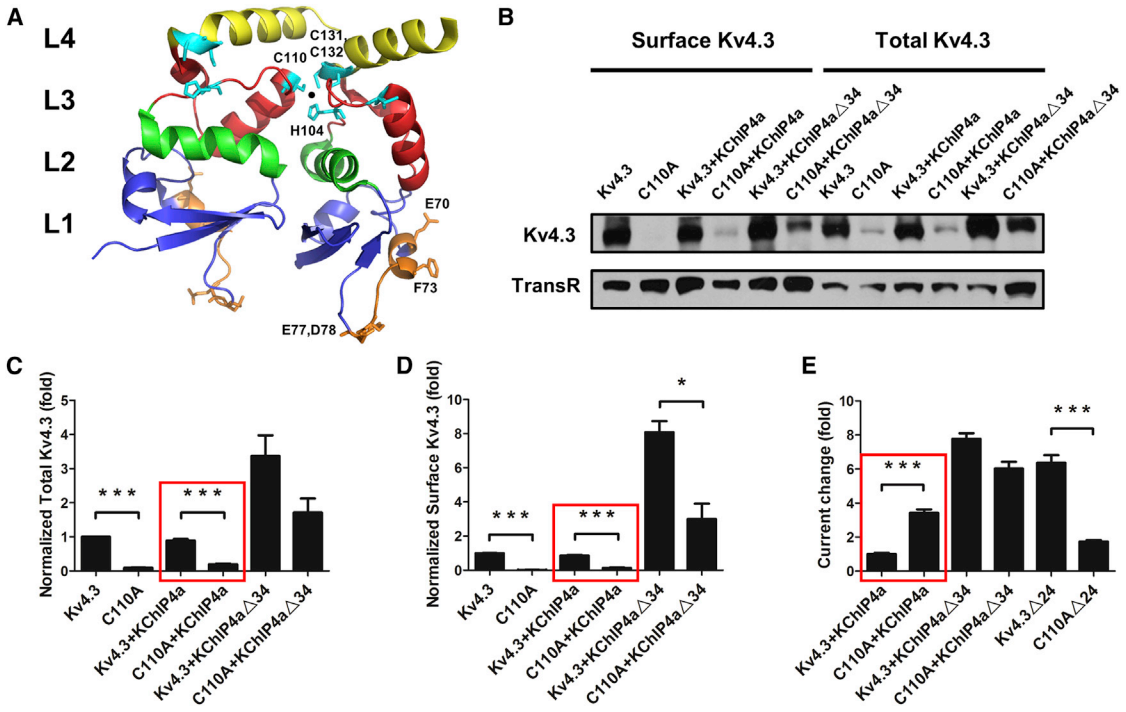

FIGURE 5 Opposite effect of C110A mutation on surface expression and current amplitude of Kv4.3 channels coexpressed with KChIP4a. (*A*) Ribbon representation of the dimeric Kv4.3 T1 domain. The four layers of the T1 scaffolding are indicated as L1–L4 in blue, green, red, and yellow, respectively. The black sphere represents the Zn^{2+} ion that is located at the T1-T1 intersubunit interface and is coordinated by a C3H1 motif. The C3H1 motif, embedded in a conserved sequence motif ($HX_5CX_{20}CC$) of the T1 domain, is indicated in cyan. The KChIP-binding residues E70, F73, E77, and D78 are shown in orange. (*B*) Western blots of total and surface proteins from HEK293T cells expressing Kv4.3, C110A, Kv4.3+KChIP4a, C110A+KChIP4a, Kv4.3+KChIP4aΔ34, or C110A+KChIP4aΔ34. (*C* and *D*) Quantitative analysis of total (*C*) and surface (*D*) expression levels of the indicated groups from *B*. Values are mean ± SEM; $n = 3$ blots; $^{***}p < 0.001$. (*E*) Normalized current recorded in oocytes expressing Kv4.3+KChIP4a, C110A+KChIP4a, Kv4.3+KChIP4aΔ34, C110A+KChIP4aΔ34, Kv4.3Δ24, or C110AΔ24. Values are mean ± SEM; $n = 11$–26 oocytes; $^{***}p < 0.001$. To see this figure in color, go online.

T1-T1 interaction, leading to destabilizing tetrameric assembly of the channel (Fig. 7, *A* and *C*). Although T1-C110A was mainly localized in the nucleus, we still could observe the KID and T1-C110A colocalization in the cytoplasm (Fig. 7 *B*). However, no FRET signal was detected in these regions (Fig. 7, *B* and *C*). These results demonstrate that the C3H1 motif of the T1 domain is critical for modulation of CSI and binding to the KChIP4a N-terminal KID.

The T1-T1 interface consisting of the C3H1 motif functions to suppress Kv4.3 CSI

To further define the role of the C3H1 motif of the T1 domain in modulating Kv4.3 CSI, we subsequently tested the inactivation kinetics of the C110A mutant. Since the C110A mutant alone is nonfunctional, we constructed a truncation of N-terminal residues 2–24 of the Kv4.3 C110A mutant (C110AΔ24) that alone is functional (35). Expression of Kv4.3Δ24 gave rise to currents in which both the CSI and SSI curves were almost identical to those of wild-type Kv4.3 (Fig. 8 *A*; Table S1), indicating that the inactivation kinetics of the N-terminal truncated Kv4.3 mutant (Kv4.3Δ24) can recapitulate the full-length Kv4.3 channel.

Further analysis showed that disrupting the C3H1 motif by mutating C110A in a truncation background (C110AΔ24) dramatically accelerated CSI, shifted the voltage dependence of SSI to a hyperpolarized direction, and slowed down the rate of recovery from inactivation (Fig. 8, *B–D*; Table S1), whereas the steady-state activation was not affected (Fig. 8 *E*). The results demonstrated that the C3H1 motif of the T1 domain functions to prevent the channel from accessing closed-inactivated states.

Sequence alignment revealed that the C3H1 motif also exists in Kv2.1 (*non-shaker*), but not in Kv1.4 (*shaker*-type; Fig. S5 A). To further confirm the role of the C3H1 motif in CSI, we replaced the Kv4.3 T1 domain with the T1 domain from either Kv1.4 (without the C3H1 motif) or Kv2.1 (with the C3H1 motif). These mutants showed the typical A-type behavior, with rapid activation of macroscopic outward currents evoked by depolarizing voltage pulses, followed by rapid inactivation (Fig. S5 B). Similarly to the C110A mutant, both the chimeric Kv4.3-T1 (Kv1.4) and Kv4.3Δ24-T1 (Kv1.4, without the C3H1 motif) exhibited enhanced CSI, a hyperpolarized shift in SSI, and slowed recovery from inactivation (Fig. 9, *A–D*; Table S1). In contrast, when we replaced the Kv4.3 T1 domain with the T1 domain from Kv2.1 (with the C3H1

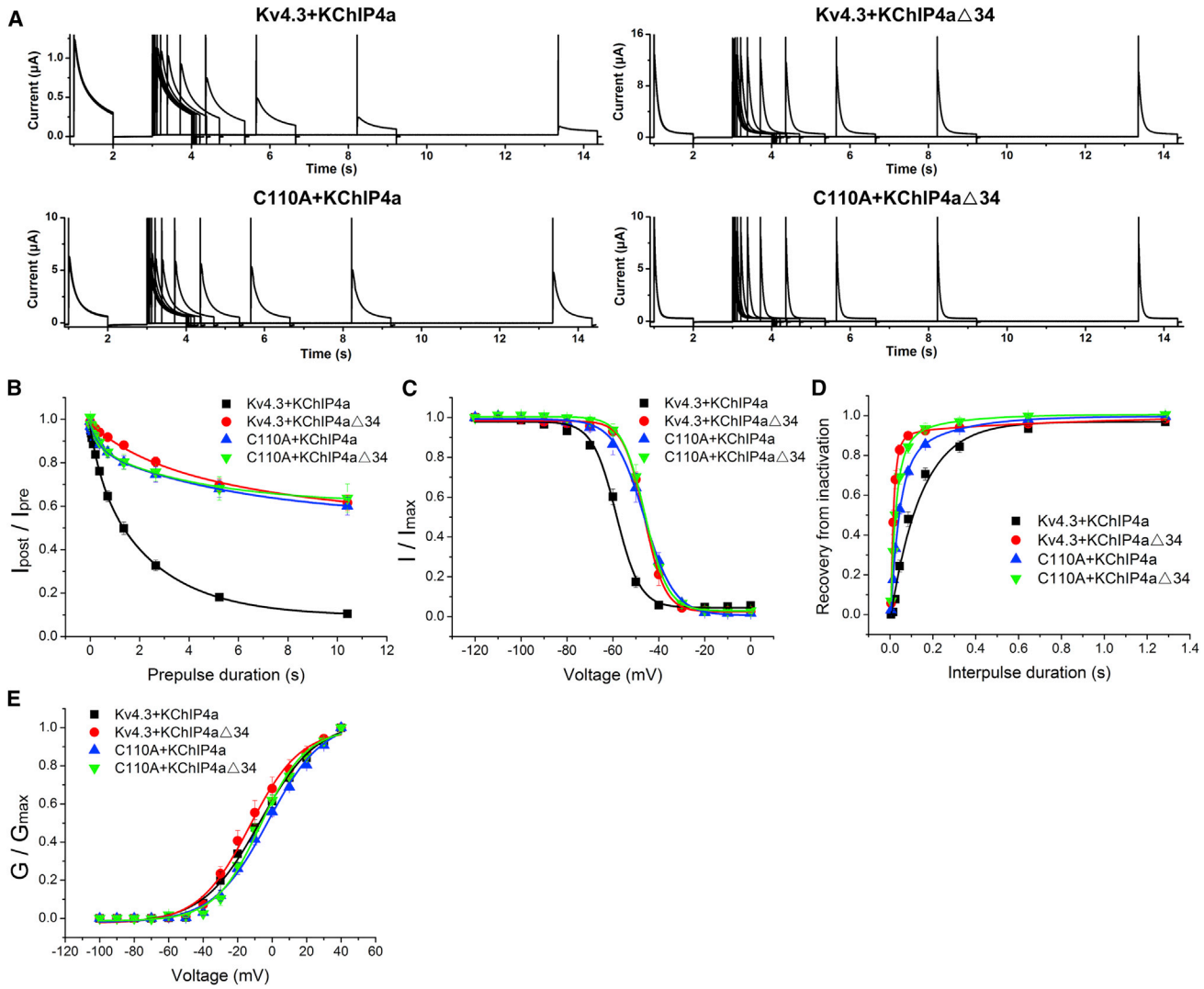

FIGURE 6 The C3H1 motif of the Kv4.3 T1 domain is critical for the KID-mediated enhancement of CSI. (*A*) Representative current traces of CSI recorded from oocytes expressing Kv4.3+KChIP4a, Kv4.3+ KChIP4aΔ34, C110A+KChIP4a, or C110A+KChIP4aΔ34. Currents were recorded at +40 mV using a double-pulse protocol with a conditioning pulse at −50 mV in variable durations (Δt) of 5 ms to 10.4 s. The current amplitudes evoked by the second pulse (+40 mV) in the protocol, relative to the amplitudes resulting from the first control pulse (I_{post}/I_{pre}), were plotted as a function of different durations of the conditioning pulses. (*B*) Analysis of CSI for Kv4.3+KChIP4a, Kv4.3+ KChIP4aΔ34, C110A+KChIP4a, or C110A+KChIP4aΔ34. (*C*) Voltage dependence of SSI for Kv4.3+KChIP4a, Kv4.3+ KChIP4aΔ34, C110A+KChIP4a, or C110A+KChIP4aΔ34. The SSI protocol consisted of a 5 s prepulse stepped from −120 mV to 0 mV in 10 mV increments, followed by a test pulse of +40 mV. The fraction of available current (I/I_{max}) was plotted against the prepulse potentials. (*D*) Steady-state activation curves of Kv4.3+KChIP4a, Kv4.3+ KChIP4aΔ34, C110A+KChIP4a, or C110A+KChIP4aΔ34. (*E*) Recovery from inactivation for Kv4.3+KChIP4a, Kv4.3+ KChIP4aΔ34, C110A+KChIP4a, or C110A+KChIP4aΔ34. Mean normalized current amplitudes were plotted as a function of interpulse duration. To see this figure in color, go online.

motif), the Kv4.3Δ24-T1 (Kv2.1) mutant showed a suppressed CSI, a depolarized shift in the voltage dependence of SSI, and accelerated recovery from inactivation (Fig. 9, *A–D*; Table S1), whereas the steady-state activation was not significantly affected by the T1 domain replacement (Fig. 9 *E*). The slower inactivation kinetics caused by Kv2.1 T1 in chimeric channels may result from the intrinsic properties of Kv2.1 T1, as both OSI and CSI of Kv2.1 are much slower than those of Kv4.3. These results indicate that the T1-T1 interface, which is characteristic of the C3H1 motif within the T1 domain and is conserved in *non-shaker* type Kv2-4 channels, plays a key role in suppressing CSI of Kv channels.

DISCUSSION

Our goal in this study was to utilize the N-terminal KID of KChIP4a as a probe to explore the molecular mechanism underlying Kv4 CSI. Our findings reveal a novel (to our knowledge) role of the T1 domain in inhibiting A-type Kv4 CSI. The T1 domain, a highly conserved cytoplasmic portion of Kv channels, not only serves as a channel

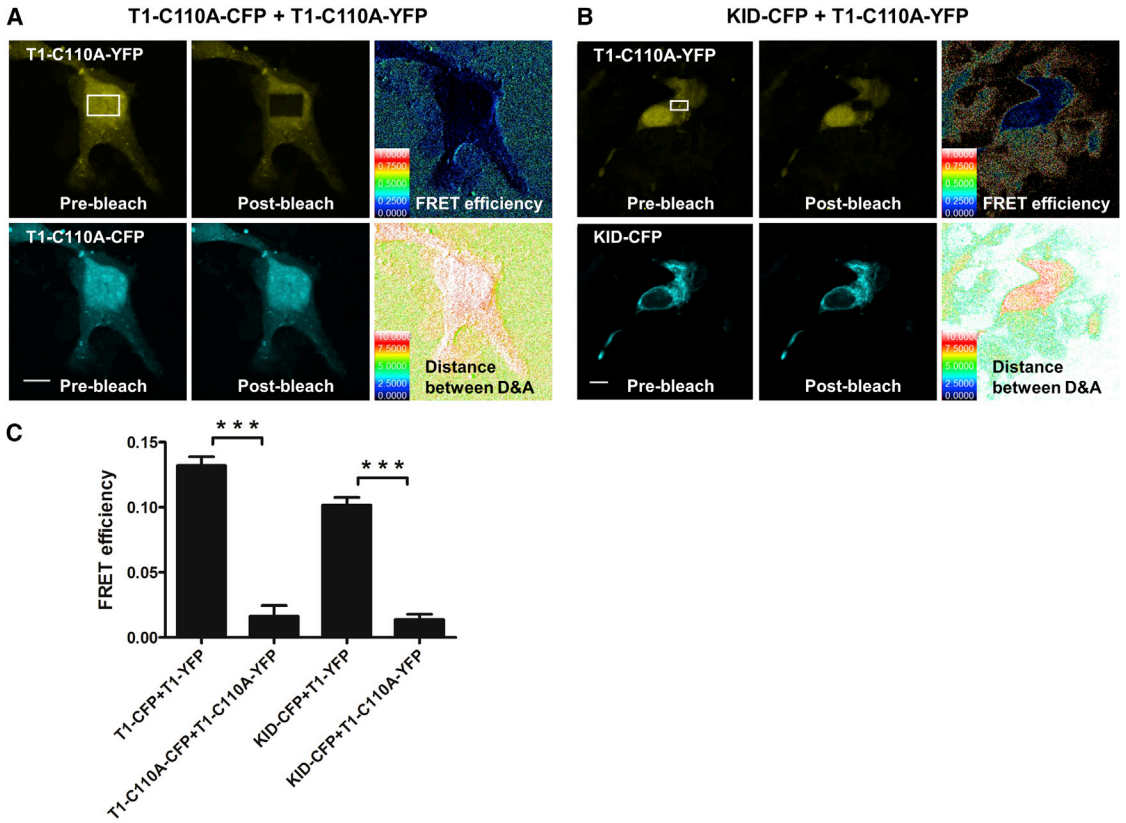

FIGURE 7 The C3H1 motif of the Kv4.3 T1 domain is critical for KID binding. (*A*) Visualization of FRET in HEK293T cells transfected with T1-C110A-CFP and T1-C110A-YFP. Images were obtained by excitation at 515 nm for YFP fluorescence (*upper-left and middle panels*) or at 456 nm for CFP fluorescence (*lower-left and middle panels*). In the upper-left panel, the region selected for photobleaching is indicated by white boxes. The upper-right panel indicates FRET efficiency and the lower-right panel indicates the distance between the donor and the acceptor. (*B*) Visualization of FRET in HEK293T cells transfected with KID-CFP and T1-C110A-YFP. (*C*) Quantitative analysis of FRET efficiency between CFP-tagged bait and YFP-tagged prey. The scale bar represents 10 μm. To see this figure in color, go online.

tetramerization domain and binding site for auxiliary subunits but also plays a crucial role in regulating channel gating. In particular, this study deepens our understanding of the role played by the T1 domain in modulating CSI of Kv4 channels.

Recently, we found that the N-terminal KID of KChIP4a exerts an inhibitory effect on channel gating by promoting CSI (27). Thus, the KID can be used as tool to probe the underlying mechanism for CSI of A-type Kv4 channels. In the first part of our study, we aimed to identify binding sites of the KID on Kv4.3 channels by utilizing FRET and BiFC two-hybrid mapping. Surprisingly, we observed a strong interaction signal between the KID and the intracellular T1 domain of Kv4.3, but not between other transmembrane fragments that were previously reported to correlate with CSI modulation. To exclude the possibility of false-negative results, we carried out experiments to demonstrate the normal expression of all channel fragments and selected regions in which CFP- and YFP-tagged peptides colocalized for further FRET analysis. However, just as in the yeast two-hybrid assay, it is still possible that the transmembrane fragments of Kv4.3 channels can become misfolded or unable to orient in the proper direction for interactions. Therefore, the weak interaction observed between the S4-S5 fragment and the KID may also result from either misfolding or improper orientation. This hypothesis could be further tested by assays such as site-specific incorporation of photo-cross-linking unnatural amino acids combined with high-resolution mass spectrometry (36,37).

The wild-type *shaker*-type Kv1 channels primarily inactivate through two classical mechanisms (both from the open state): N-type and P/C-type inactivation. Interestingly, an alternatively spliced short isoform of Kv1.5 (Kv1.5ΔN209), which results in disruption of the T1 domain, exhibits a U-type inactivation that differs from the full-length Kv1.5 and is very similar to that observed in Kv2.1 (38–40). The feature of U-type inactivation is consistent with preferential CSI because the prepulse inactivation curve displays a deep inactivation at intermediate voltages and progressively less inactivation at more positive voltages. Furthermore, disruption of the intersubunit T1 interface by mutating residues E131 and T132 of either Kv1.5 or Kv1.2 to alanines leads to a similar change (39), indicating that the T1 domain serves as a switch to control

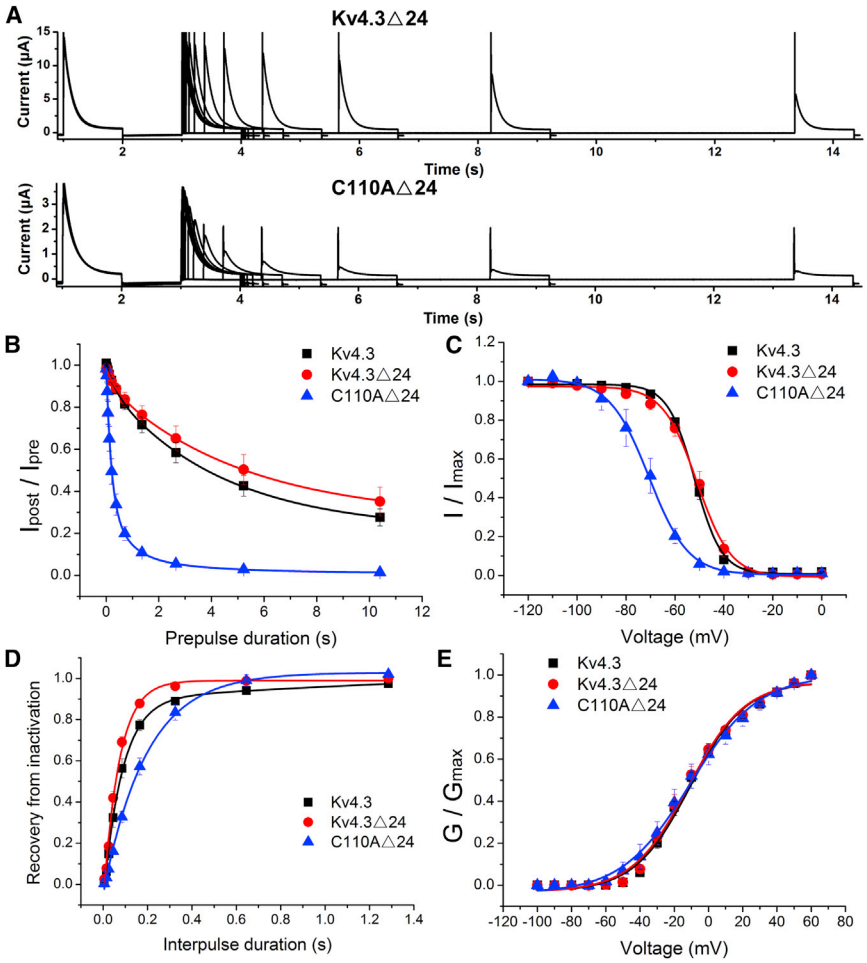

FIGURE 8 Disrupting the T1-T1 interface consisting of the C3H1 motif facilitates CSI of Kv4.3 channels. (*A*) Representative current traces of CSI recorded from oocytes expressing Kv4.3Δ24 or C110AΔ24. Currents were recorded at +40 mV using a double-pulse protocol with a conditioning pulse at −50 mV in variable durations (Δt) of 5 ms to 10.4 s. The current amplitudes evoked by the second pulse (+40 mV) in the protocol, relative to the amplitudes resulting from the first control pulse (I_{post}/I_{pre}), were plotted as a function of different durations of the conditioning pulses. (*B*) Analysis for CSI of Kv4.3, Kv4.3Δ24, and C110AΔ24. (*C*) Voltage dependence of SSI of Kv4.3, Kv4.3Δ24, or C110AΔ24. The SSI protocol consisted of a 5 s prepulse stepped from −120 mV to 0 mV in 10 mV increments, followed by a test pulse of +40 mV. The fraction of available current (I/I_{max}) was plotted against the prepulse potentials. (*D*) Steady state-activation curve of Kv4.3, Kv4.3Δ24, or C110AΔ24. (*E*) Recovery from inactivation for Kv4.3, Kv4.3Δ24, or C110AΔ24. Mean normalized current amplitudes were plotted as a function of interpulse duration. To see this figure in color, go online.

the conformational changes underlying CSI. Restoration of the wild-type inactivation properties of Kv1.5 by fusing the T1 domain from Kv1.1 or Kv1.3 channels to the Kv1.5 N-terminal truncation further supports an evolutionary conserved and generalized role of the T1 domain in the regulation of CSI (39).

In contrast to full-length Kv1 (*Shaker*) channels, Kv2-4 (*non-Shaker*) channels undergo prominent CSI (3,41,42). For Kv4 channels, it has been demonstrated that the T1-T1 intersubunit interface around the C3H1 high-affinity Zn^{2+}-binding site (coordinated by residues H104, C110, C131, and C132) is functionally active and dynamic during channel gating (16). Since the Zn^{2+}-binding cysteines (C110, C131, and C132) have reactive thiolate groups, modification by thiol-specific reagents such as MTSET can cause irreversible inhibition of Kv4 channels by interfering with the gating kinetics, but not with tetramer dissociation (16). The rate constant of inhibition by MTSET is faster when MTSET is applied to channels in the activated state as compared with resting and inactivated channels (17). Since CSI occurs in the partially activated closed state and is highly coupled to channel activation gating, MTSET-mediated Kv4 inhibition through effects on the T1 domain may also result from enhanced CSI. Besides MTSET modification, the formation of a disulfide bridge between C110 and C132 induced by nitric oxide, which prevents structural rearrangement of the C3H1 motif, also profoundly inhibits Kv4 channel activity, and this inhibition can be reversed by reduced glutathione and suppressed by intracellular Zn^{2+} (43). Together with our data, these results indicate that the dynamic conformation and rearrangement of the C3H1 motif is crucial for regulating CSI, and KChIP4a N-terminal KID binding to the T1 domain may induce local conformational changes in the T1-T1 intersubunit interface consisting of the C3H1 motif in a manner similar to MTSET modification or oxidation of T1 cysteines, thus interfering with the T1-domain-mediated inhibition of CSI.

According to the crystal structure of the Kv4.3-T1 domain (13), the T1 scaffolding can be divided into four layers (L1–L4 in Fig. 5 *A*). In the intact channel, L4 is directly connected to the T1-S1 linker, and the Zn^{2+}-binding site is located between L3 and L4 in a region that is probably close to the transmembrane core of the channel (44). Based on work with Kv4.1 channels, it has been concluded that the complex voltage-dependent gating rearrangements include propagated movements in the conserved

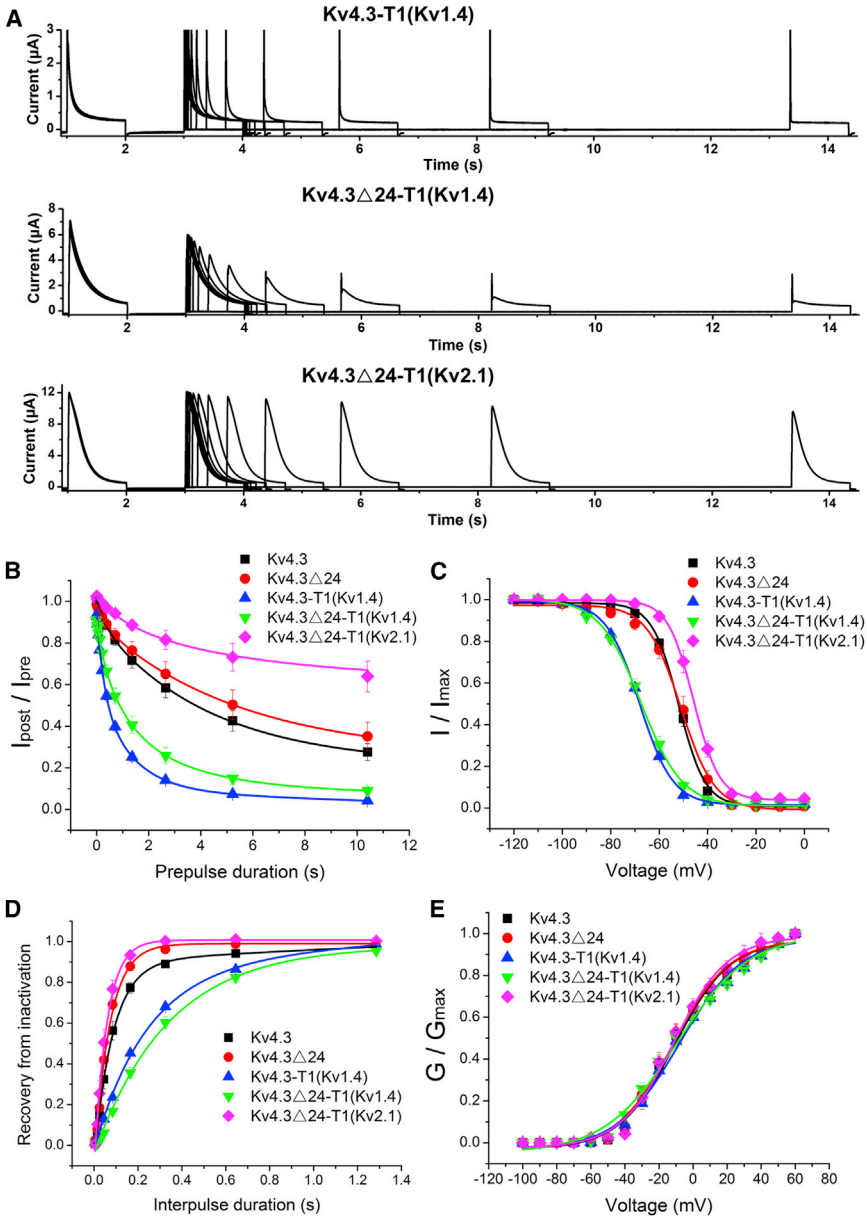

FIGURE 9 The T1-T1 interface consisting of the C3H1 motif suppresses CSI of Kv4.3 channels. (*A*) Representative current traces of CSI recorded from oocytes expressing Kv4.3-T1 (Kv1.4), Kv4.3Δ24-T1 (Kv1.4), or Kv4.3Δ24-T1 (Kv2.1). Currents were recorded at +40 mV using a double-pulse protocol with a conditioning pulse at −50 mV in variable durations (Δt) of 5 ms to 10.4 s. The current amplitudes evoked by the second pulse (+40 mV) in the protocol, relative to the amplitudes resulting from the first control pulse (I_{post}/I_{pre}), were plotted as a function of different durations of the conditioning pulses. (*B*) Analysis for CSI of Kv4.3, Kv4.3Δ24, Kv4.3-T1 (Kv1.4), Kv4.3Δ24-T1 (Kv1.4), or Kv4.3Δ24-T1 (Kv2.1). (*C*) Voltage dependence of SSI of Kv4.3, Kv4.3Δ24, Kv4.3-T1 (Kv1.4), Kv4.3Δ24-T1 (Kv1.4), or Kv4.3Δ24-T1 (Kv2.1). The SSI protocol consisted of a 5 s prepulse stepped from −120 mV to 0 mV in 10-mV increment, followed by a test pulse of +40 mV. The fraction of available current (I/I_{max}) was plotted against the prepulse potentials. (*D*) Steady-state activation curve of Kv4.3, Kv4.3Δ24, Kv4.3-T1 (Kv1.4), Kv4.3Δ24-T1 (Kv1.4), or Kv4.3Δ24-T1 (Kv2.1). (*E*) Recovery from inactivation for Kv4.3, Kv4.3Δ24, Kv4.3-T1 (Kv1.4), Kv4.3Δ24-T1 (Kv1.4), or Kv4.3Δ24-T1 (Kv2.1). Mean normalized current amplitudes were plotted as a function of interpulse duration. To see this figure in color, go online.

L4 layer of the T1 domain and a post-S6 C-terminal segment (activation gate) that may form a direct contact with the T1 domain (17). In this study, we show that both the Kv4.3 C110A mutant and the Kv4.3-T1 (Kv1.4, without the C3H1 motif) chimera accelerate CSI, indicating that the distinct conformation of the T1 domain, especially the part of the interfacial Zn^{2+}-binding site composed of the C3H1 motif, is highly involved in suppressing CSI. In contrast, replacement of the Kv4.3 T1 domain with the Kv2.1 T1 domain (with the C3H1 motif) functions like the coexpression with KChIP4a core to prevent CSI, further supporting a general role of the C3H1 motif in suppression of CSI in *non-Shaker*-type Kv channels. Our findings raise the possibility that the C3H1 motif or its adjacent region in the T1 domain may directly interact with the post-S6 C-terminal segment, and this stable interaction likely allows the T1 domain to stabilize the connection between the S4 voltage-sensing domain and the intracellular S6 activation gate. Therefore, disrupting the C3H1 motif likely results in decoupling of the T1 domain from the S6 extension, leading to acceleration of Kv4.3 CSI and inhibition of channel function. There is also evidence suggesting that CSI in Kv4 channels is due to slow and profound gating charge (Q) immobilization at hyperpolarized voltages before the channel opens (45). It is possible that the voltage-dependent rearrangement in the intracellular C3H1 motif of the T1 domain in turn regulates the slow rearrangement of the voltage sensor.

In their original description of KChIP4a, Holmqvist et al. (22) did not report any obvious change in CSI and SSI of

Kv4.3 coexpressed with KChIP4a in several cell types, including cerebellar granule neurons. We suspect that this difference between their study and ours likely reflects the fact that the C-terminal KChIP4a core used in their study functions to suppress CSI, thereby counteracting the CSI-promoting effect of its N-terminal KID. In addition, the modulation of Kv4 CSI or SSI by full-length KChIP4a may not be obvious under certain experimental conditions. For instance, the CSI and SSI kinetics of Kv4.3 alone is not much different from that of Kv4.3 coexpressed with KChIP4a (Fig. S1; Table S2). In neurons, Kv4 α subunits interact with auxiliary subunits to form macromolecular K^+ channel complexes. Different KChIPs can bind to Kv4 channels via their conserved core domain and produce variable effects on Kv4 channel function. Therefore, comparing current densities and gating properties of Kv4 channel complexes with different KChIPs can likely reveal distinct effects of individual KChIPs on the dynamic modulation of Kv4 channel function.

Numerous studies have demonstrated that the common core of KChIPs alone is sufficient to function as full-length KChIPs and promote Kv4 trafficking. Two binding sites for the KChIP core have been identified within Kv4 channels: the distal N-terminus and the T1 domain (13,20,21). As Kv4.3 N-terminal deletion does not significantly alter the CSI kinetics of Kv4.3, we propose that the interaction between the KChIP core and the T1 domain is responsible for the KChIP core-mediated inhibition of CSI, which likely results from T1-T1 stabilization facilitated by the KChIP core. The observations that the KChIP core can functionally rescue C110A mutant channels by a clamping action (21,35,46), and the CSI kinetics of the C110A/KChIP core is identical to that of wild-type Kv4.3 further support our hypothesis that conformational stabilization of the T1-T1 interface is critical for suppressing CSI. As mentioned above, internally applying nitric oxide to induce disulfide cross-linking between C110 and C132 also profoundly inhibits Kv4.1 channel activity, suggesting that not only the stability but also the mobility and dynamics of the T1-T1 interface are crucial for its gating role. Similarly to the T1 domain, the conserved KChIP core enhances Kv4 channel function by promoting tetrameric assembly as well as by stabilizing the coupling between voltage-dependent activation and conformational changes involved in the intracellular T1-T1 interface. Furthermore, since different KChIPs contain a highly conserved C-terminal core domain that binds to both the distal N-terminus and the T1 domain of Kv4 channels, our findings offer an explanation for the discrepancies between surface expression levels of Kv4.2 regulated by KChIP2 and their current amplitudes previously reported by Foeger et al. (47).

Interestingly, although the C110A mutant alone displays loss-of-function as a result of misassembly, the N-terminal deletion C110AΔ24 mutant can give rise to a functional current without coexpression of KChIPs. Previous studies have demonstrated that Kv4 N-terminal truncations increase Kv4 currents, partially by mimicking the effects of coexpression of KChIPs (KChIP1-3) (47–49). There are two possible explanations for the increase of Kv4 currents. One is that the N-terminus of Kv4 channels, which contains an endoplasmic reticulum retention motif, can be masked by the KChIP core, and therefore deleting the N-terminus can result in increased surface expression of Kv4 channels (48). Foeger et al. (47) suggested that Kv4 N-terminal truncation-induced augmentation of Kv4 currents likely results from changes in channel gating, since they observed no increase in the total or surface expression levels of Kv4 channels. In our study, we found that Kv4 N-terminal deletion (Kv4.3Δ24) moderately suppressed CSI and rescued the Kv4 channel tetramerization-deficient mutant (C110AΔ24). This suggests that the Kv4 N-terminus probably contains a distinct domain that inhibits channel assembly, and therefore that deleting the N-terminus promotes channel tetramerization.

A growing body of evidence suggests that CSI plays an important role in ion channel physiology and function. This inactivation phenomenon was first described in Nav channels (50–52) but has been demonstrated in other widely studied Cav (53–55), Kv (3,39,41,42), BK (56), and HCN channels (57), as well as in ligand-gated ion channels such as NMDA receptors (termed desensitization) (58). This suggests that CSI/desensitization may be a more generalized feature of ion channels than was previously thought. Although the fundamental conformational changes underlying CSI remain elusive, the cytosolic T1 domain of Kv channels appears to be intimately involved in the regulation of CSI properties. As a docking site for a number of intracellular regulatory molecules, the T1 domain may provide an important mechanism for transient and stable alterations of both the activation and inactivation kinetics of Kv channels.

SUPPORTING MATERIAL

Five figures and two tables are available at http://www.biophysj.org/biophysj/supplemental/S0006-3495(14)00783-8.

We thank our previous laboratory member Ping Liang for discussion. K.W. thanks J.M. Wang for her consistent support during this research.

This work was supported by research grants to K.W. from the National Science Foundation of China (31370741), the Ministry of Science and Technology of China (2013CB531302), the National Science Foundation of China (81221002), and the Ministry of Education of China (111 Project, B07001). Y.-Q.T. and K.W. conceived and designed experiments; Y.-Q.T., J.-H.Z., F.Y., and J.Z. performed experiments and analyzed the data; and Y.-Q.T. and K.W. wrote the manuscript.

REFERENCES

1. Bähring, R., and M. Covarrubias. 2011. Mechanisms of closed-state inactivation in voltage-gated ion channels. *J. Physiol.* 589:461–479.

2. Jerng, H. H., M. Shahidullah, and M. Covarrubias. 1999. Inactivation gating of Kv4 potassium channels: molecular interactions involving the inner vestibule of the pore. *J. Gen. Physiol.* 113:641–660.
3. Bähring, R., L. M. Boland, …, O. Pongs. 2001. Kinetic analysis of open- and closed-state inactivation transitions in human Kv4.2 A-type potassium channels. *J. Physiol.* 535:65–81.
4. Alonso, G., and H. Widmer. 1997. Clustering of KV4.2 potassium channels in postsynaptic membrane of rat supraoptic neurons: an ultrastructural study. *Neuroscience.* 77:617–621.
5. Schoppa, N. E., and G. L. Westbrook. 1999. Regulation of synaptic timing in the olfactory bulb by an A-type potassium current. *Nat. Neurosci.* 2:1106–1113.
6. Ramakers, G. M., and J. F. Storm. 2002. A postsynaptic transient K(+) current modulated by arachidonic acid regulates synaptic integration and threshold for LTP induction in hippocampal pyramidal cells. *Proc. Natl. Acad. Sci. USA.* 99:10144–10149.
7. Watanabe, S., D. A. Hoffman, …, D. Johnston. 2002. Dendritic K+ channels contribute to spike-timing dependent long-term potentiation in hippocampal pyramidal neurons. *Proc. Natl. Acad. Sci. USA.* 99: 8366–8371.
8. Cai, X., C. W. Liang, …, S. M. Thompson. 2004. Unique roles of SK and Kv4.2 potassium channels in dendritic integration. *Neuron.* 44: 351–364.
9. Chen, X., L. L. Yuan, …, D. Johnston. 2006. Deletion of Kv4.2 gene eliminates dendritic A-type K+ current and enhances induction of long-term potentiation in hippocampal CA1 pyramidal neurons. *J. Neurosci.* 26:12143–12151.
10. Long, S. B., E. B. Campbell, and R. Mackinnon. 2005. Crystal structure of a mammalian voltage-dependent Shaker family K+ channel. *Science.* 309:897–903.
11. Bixby, K. A., M. H. Nanao, …, S. Choe. 1999. Zn2+-binding and molecular determinants of tetramerization in voltage-gated K+ channels. *Nat. Struct. Biol.* 6:38–43.
12. Jahng, A. W., C. Strang, …, S. Choe. 2002. Zinc mediates assembly of the T1 domain of the voltage-gated K channel 4.2. *J. Biol. Chem.* 277:47885–47890.
13. Scannevin, R. H., K. Wang, …, K. J. Rhodes. 2004. Two N-terminal domains of Kv4 K(+) channels regulate binding to and modulation by KChIP1. *Neuron.* 41:587–598.
14. Cushman, S. J., M. H. Nanao, …, P. J. Pfaffinger. 2000. Voltage dependent activation of potassium channels is coupled to T1 domain structure. *Nat. Struct. Biol.* 7:403–407.
15. Minor, D. L., Y. F. Lin, …, J. M. Berger. 2000. The polar T1 interface is linked to conformational changes that open the voltage-gated potassium channel. *Cell.* 102:657–670.
16. Wang, G., M. Shahidullah, …, M. Covarrubias. 2005. Functionally active t1-t1 interfaces revealed by the accessibility of intracellular thiolate groups in kv4 channels. *J. Gen. Physiol.* 126:55–69.
17. Wang, G., and M. Covarrubias. 2006. Voltage-dependent gating rearrangements in the intracellular T1-T1 interface of a K+ channel. *J. Gen. Physiol.* 127:391–400.
18. Gulbis, J. M., M. Zhou, …, R. MacKinnon. 2000. Structure of the cytoplasmic beta subunit-T1 assembly of voltage-dependent K+ channels. *Science.* 289:123–127.
19. An, W. F., M. R. Bowlby, …, K. J. Rhodes. 2000. Modulation of A-type potassium channels by a family of calcium sensors. *Nature.* 403: 553–556.
20. Pioletti, M., F. Findeisen, …, D. L. Minor, Jr. 2006. Three-dimensional structure of the KChIP1-Kv4.3 T1 complex reveals a cross-shaped octamer. *Nat. Struct. Mol. Biol.* 13:987–995.
21. Wang, H., Y. Yan, …, J. Chai. 2007. Structural basis for modulation of Kv4 K+ channels by auxiliary KChIP subunits. *Nat. Neurosci.* 10: 32–39.
22. Holmqvist, M. H., J. Cao, …, W. F. An. 2002. Elimination of fast inactivation in Kv4 A-type potassium channels by an auxiliary subunit domain. *Proc. Natl. Acad. Sci. USA.* 99:1035–1040.
23. Takimoto, K., E. K. Yang, and L. Conforti. 2002. Palmitoylation of KChIP splicing variants is required for efficient cell surface expression of Kv4.3 channels. *J. Biol. Chem.* 277:26904–26911.
24. Boland, L. M., M. Jiang, …, S. M. O'Grady. 2003. Functional properties of a brain-specific NH2-terminally spliced modulator of Kv4 channels. *Am. J. Physiol. Cell Physiol.* 285:C161–C170.
25. Van Hoorick, D., A. Raes, and D. J. Snyders. 2007. The aromatic cluster in KCHIP1b affects Kv4 inactivation gating. *J. Physiol.* 583: 959–969.
26. Liang, P., H. Wang, …, K. Wang. 2009. Structural insights into KChIP4a modulation of Kv4.3 inactivation. *J. Biol. Chem.* 284: 4960–4967.
27. Tang, Y. Q., P. Liang, …, K. Wang. 2013. Auxiliary KChIP4a suppresses A-type K+ current through endoplasmic reticulum (ER) retention and promoting closed-state inactivation of Kv4 channels. *J. Biol. Chem.* 288:14727–14741.
28. Erickson, M. G., H. Liang, …, D. T. Yue. 2003. FRET two-hybrid mapping reveals function and location of L-type Ca2+ channel CaM preassociation. *Neuron.* 39:97–107.
29. Skerritt, M. R., and D. L. Campbell. 2007. Role of S4 positively charged residues in the regulation of Kv4.3 inactivation and recovery. *Am. J. Physiol. Cell Physiol.* 293:C906–C914.
30. Skerritt, M. R., and D. L. Campbell. 2008. Non-native R1 substitution in the s4 domain uniquely alters Kv4.3 channel gating. *PLoS ONE.* 3:e3773.
31. Barghaan, J., and R. Bähring. 2009. Dynamic coupling of voltage sensor and gate involved in closed-state inactivation of kv4.2 channels. *J. Gen. Physiol.* 133:205–224.
32. Skerritt, M. R., and D. L. Campbell. 2009. Contribution of electrostatic and structural properties of Kv4.3 S4 arginine residues to the regulation of channel gating. *Biochim. Biophys. Acta.* 1788:458–469.
33. Shyu, Y. J., C. D. Suarez, and C. D. Hu. 2008. Visualization of ternary complexes in living cells by using a BiFC-based FRET assay. *Nat. Protoc.* 3:1693–1702.
34. Hu, C. D., Y. Chinenov, and T. K. Kerppola. 2002. Visualization of interactions among bZIP and Rel family proteins in living cells using bimolecular fluorescence complementation. *Mol. Cell.* 9:789–798.
35. Liang, P., H. Chen, …, K. Wang. 2010. Functional rescue of Kv4.3 channel tetramerization mutants by KChIP4a. *Biophys. J.* 98:2867–2876.
36. Pless, S. A., and C. A. Ahern. 2013. Unnatural amino acids as probes of ligand-receptor interactions and their conformational consequences. *Annu. Rev. Pharmacol. Toxicol.* 53:211–229.
37. Hino, N., Y. Okazaki, …, S. Yokoyama. 2005. Protein photo-cross-linking in mammalian cells by site-specific incorporation of a photoreactive amino acid. *Nat. Methods.* 2:201–206.
38. Kurata, H. T., G. S. Soon, and D. Fedida. 2001. Altered state dependence of c-type inactivation in the long and short forms of human Kv1.5. *J. Gen. Physiol.* 118:315–332.
39. Kurata, H. T., G. S. Soon, …, D. Fedida. 2002. Amino-terminal determinants of U-type inactivation of voltage-gated K+ channels. *J. Biol. Chem.* 277:29045–29053.
40. Kurata, H. T., K. W. Doerksen, …, D. Fedida. 2005. Separation of P/C- and U-type inactivation pathways in Kv1.5 potassium channels. *J. Physiol.* 568:31–46.
41. Klemic, K. G., C. C. Shieh, …, S. W. Jones. 1998. Inactivation of Kv2.1 potassium channels. *Biophys. J.* 74:1779–1789.
42. Klemic, K. G., G. E. Kirsch, and S. W. Jones. 2001. U-type inactivation of Kv3.1 and Shaker potassium channels. *Biophys. J.* 81:814–826.
43. Wang, G., C. Strang, …, M. Covarrubias. 2007. Zn2+-dependent redox switch in the intracellular T1-T1 interface of a Kv channel. *J. Biol. Chem.* 282:13637–13647.
44. Kim, L. A., J. Furst, …, N. Grigorieff. 2004. Three-dimensional structure of I(to); Kv4.2-KChIP2 ion channels by electron microscopy at 21 Angstrom resolution. *Neuron.* 41:513–519.

45. Dougherty, K., J. A. De Santiago-Castillo, and M. Covarrubias. 2008. Gating charge immobilization in Kv4.2 channels: the basis of closed-state inactivation. *J. Gen. Physiol.* 131:257–273.

46. Kunjilwar, K., C. Strang, …, P. J. Pfaffinger. 2004. KChIP3 rescues the functional expression of Shal channel tetramerization mutants. *J. Biol. Chem.* 279:54542–54551.

47. Foeger, N. C., C. Marionneau, and J. M. Nerbonne. 2010. Co-assembly of Kv4 alpha subunits with K+ channel-interacting protein 2 stabilizes protein expression and promotes surface retention of channel complexes. *J. Biol. Chem.* 285:33413–33422.

48. Bähring, R., J. Dannenberg, …, D. Isbrandt. 2001. Conserved Kv4 N-terminal domain critical for effects of Kv channel-interacting protein 2.2 on channel expression and gating. *J. Biol. Chem.* 276:23888–23894.

49. Salvador-Recatalà, V., W. J. Gallin, …, A. N. Spencer. 2006. A potassium channel (Kv4) cloned from the heart of the tunicate Ciona intestinalis and its modulation by a KChIP subunit. *J. Exp. Biol.* 209: 731–747.

50. Bean, B. P. 1981. Sodium channel inactivation in the crayfish giant axon. Must channels open before inactivating? *Biophys. J.* 35:595–614.

51. Aldrich, R. W., and C. F. Stevens. 1983. Inactivation of open and closed sodium channels determined separately. *Cold Spring Harb. Symp. Quant. Biol.* 48:147–153.

52. Armstrong, C. M. 2006. Na channel inactivation from open and closed states. *Proc. Natl. Acad. Sci. USA.* 103:17991–17996.

53. Patil, P. G., D. L. Brody, and D. T. Yue. 1998. Preferential closed-state inactivation of neuronal calcium channels. *Neuron.* 20:1027–1038.

54. Jones, L. P., C. D. DeMaria, and D. T. Yue. 1999. N-type calcium channel inactivation probed by gating-current analysis. *Biophys. J.* 76: 2530–2552.

55. Thaler, C., A. C. Gray, and D. Lipscombe. 2004. Cumulative inactivation of N-type CaV2.2 calcium channels modified by alternative splicing. *Proc. Natl. Acad. Sci. USA.* 101:5675–5679.

56. Ding, J. P., and C. J. Lingle. 2002. Steady-state and closed-state inactivation properties of inactivating BK channels. *Biophys. J.* 82:2448–2465.

57. Shin, K. S., C. Maertens, …, G. Yellen. 2004. Inactivation in HCN channels results from reclosure of the activation gate: desensitization to voltage. *Neuron.* 41:737–744.

58. Lin, F., and C. F. Stevens. 1994. Both open and closed NMDA receptor channels desensitize. *J. Neurosci.* 14:2153–2160.